Lab on a Chip

Check for updates

Long-term flow through human intestinal organoids with the gut organoid flow chip (GOFlowChip)†

Barkan Sidar, [iD] [ab] Brittany R. Jenkins, [iD] [c] Sha Huang, [d] Jason R. Spence, [iD] *[de]
Seth T. Walk*[c] and James N. Wilking [iD] *[ab]

Human intestinal organoids (HIOs) are millimeter-scale models of the human intestinal epithelium and hold tremendous potential for advancing fundamental and applied biomedical research. HIOs resemble the native gut in that they consist of a fluid-filled lumen surrounded by a polarized epithelium and associated mesenchyme; however, their topologically-closed, spherical shape prevents flow through the interior luminal space, making the system less physiological and leading to the buildup of cellular and metabolic waste. These factors ultimately limit experimentation inside the HIOs. Here, we present a millifluidic device called the gut organoid flow chip (GOFlowChip), which we use to "port" HIOs and establish steady-state liquid flow through the lumen for multiple days. This long-term flow is enabled by the use of laser-cut silicone gaskets, which allow liquid in the device to be slightly pressurized, suppressing bubble formation. To demonstrate the utility of the device, we establish separate luminal and extraluminal flow and use luminal flow to remove accumulated waste. This represents the first demonstration of established liquid flow through the luminal space of a gastrointestinal organoid over physiologically relevant time scales. Flow cytometry results reveal that HIO cell viability is unaffected by long-term porting and luminal flow. We expect the real-time, long-term control over luminal and extraluminal contents provided by the GOFlowChip will enable a wide variety of studies including intestinal secretion, absorption, transport, and co-culture with intestinal microorganisms.

[a] *Department of Chemical and Biological Engineering, Montana State University, Bozeman, MT, USA. E-mail: jwilking@gmail.com*
[b] *Center for Biofilm Engineering, Montana State University, Bozeman, MT, USA*
[c] *Department of Microbiology & Immunology, Montana State University, Bozeman, MT, USA. E-mail: seth.t.walk@gmail.com*
[d] *Department of Internal Medicine, Division of Gastroenterology, University of Michigan, Ann Arbor, MI, USA. E-mail: spencejr@umich.edu*
[e] *Department of Cell and Developmental Biology, University of Michigan, Ann Arbor, MI, USA*
† Electronic supplementary information (ESI) available. See DOI: 10.1039/c9lc00653b

Introduction

Human intestinal organoids (HIOs) are millimeter-scale experimental models of the intestinal epithelium.[1–3] These tissues are grown in the lab through directed differentiation of human pluripotent stem cells (iPSC)[1] and have become a standard for basic and applied biomedical research.[3–13] HIOs are spherical in shape and consist of an inner, liquid-filled space enclosed by a polarized epithelial shell that mimics the cellular complexity of the intestinal epithelium. The shell is comprised of several epithelial lineages, including stem cells, progenitors, and absorptive enterocytes, as well as secretory goblet, enteroendocrine, and Paneth cell precursors.[1,14] These cells are bound to one another through tight junctions and thus provide a physical barrier between the lumen and the outside environment. As in the human gut, the HIO barrier is dynamic and both actively and passively mediates the transport of molecules and water.[15–17] Quite remarkably, HIOs exist as topologically closed, self-contained systems for human gut research.

HIOs are particularly useful for studying interactions between bacteria and human host tissue. For example, the natural microbial colonization of immature intestinal epithelium, such as that in newborn infants, has been modeled by co-culturing microorganisms inside HIOs[3]. HIOs also represent a new and unconventional model for understanding enteric dysfunction, which can be caused by pathogenic bacteria and viruses.[10–12] To study such interactions, microbes have been injected into the luminal space using a micropipette.[3,10–12] After injection, the epithelial shell rapidly heals, and both HIO and microbes can be cultured together. The topologically closed surface of the epithelial shell is beneficial in that it acts to contain the microorganisms, thus allowing for short-term assays. However, the human gut is not a closed system and transport

into and out of the intestine is critical to clear human and microbial cellular waste. The lack of liquid advection through the luminal space in HIOs and other gastrointestinal organoids leads to a buildup of waste and cellular debris that can eventually lead to "popping" events.[18] Thus, enclosed HIOs do not adequately mimic natural luminal flow through the human gut.

Short-term luminal flow has been established through human gastric organoids (HGOs) for tens of minutes;[19] however, to perform physiologically relevant experiments such as real-time monitoring and control of luminal contents, luminal flow must be established for multiple days, and extending flow time by more than two orders of magnitude presents significant engineering challenges. For example, the flow of biological media in millifluidic devices is plagued by the formation of bubbles, which disrupt the luminal space and interfere with organoid imaging.[20] Moreover, luminal waste that dislodges during long-term flow leads to device clogging. These issues preclude long-term imaging and require new engineering solutions. Without a fluidic system that better reflects *in vivo* conditions with controlled luminal flow over multiple days, new avenues of long-term experimentation involving gastrointestinal organoids will be limited.

Here, we present a multilayer millifluidic device used to establish long-term internal liquid HIO flow in parallel with external flow around the outer surface of the HIO. We call this device the gut organoid flow chip (GOFlowChip). Internal liquid flow allows for the removal of accumulated waste from the lumen, while the extraluminal flow exchanges nutrients and waste to mimic collection by mesenteric arteries and portal vein transport. Luminal flow through the organoid is provided by tapered glass capillaries, which are used to puncture the HIO and establish flow for periods as long as $t = 65$ h. This long-term flow is enabled by the use of laser-cut silicone gaskets, which allow liquid in the device to be slightly pressurized, suppressing bubble formation. Flow around the outside of the organoid is provided by an additional channel cut into the device. The seal which forms at each puncture site is sufficient to maintain separation between the inner and outer contents of the organoid under physiologically relevant flow conditions. This device can be used for a broad range of experimentation and imaging. For example, independent control of luminal and extra-luminal liquid flow allows for the introduction of molecules or colloidal-scale objects, such as bacteria, into the luminal space. Additionally, fine-scale control of HIO luminal flow will enable continuous sampling of the luminal contents.

Background

HIOs are routinely grown from stem cells into multi-lineage, millimeter-scale, enclosed spheres with an internal lumen (Fig. 1A).[1,2] The spheres are generated and propagated within a bio-compatible hydrogel,[21–23] and during growth are exposed to growth factors necessary for cellular
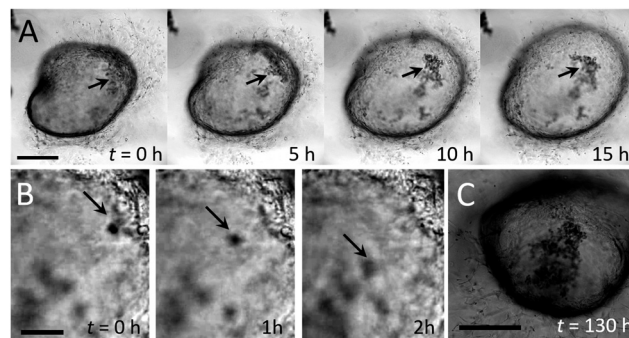

Fig. 1 Time-lapse microscopy imaging of a human intestinal organoid (HIO) reveals waste accumulation. (A) Image series. Closed-shell structure formed by an HIO. The epithelial sheet acts as semipermeable membrane, limiting transport between the luminal and extraluminal space. In the early stages of organoid growth, HIOs are optically transparent, but cellular debris accumulates over time (black arrows). Scale bar represents 1 mm. (B) Image series. High magnification time-lapse images of small debris (black arrows) sloughing off the inner surface and settling to the bottom of the interior space. Images are separated by 1 h each. Scale bar represents 0.1 mm. (C) After 130 h, the HIO from (A) has darkened significantly and waste has continued to accumulate in the luminal space.

differentiation and proliferation.[13] HIOs are considered fully differentiated once they have reached several millimeters in diameter, which requires six to eight weeks of growth. Functional and physiological assays conducted on HIOs at this stage reveal the presence of brush borders on enterocytes, production of mucin by goblet cells, peptide transport systems, and barrier-forming tight junctions.[13,24] HIOs older than eight weeks become dense with accumulated waste and the epithelial shell can lose mechanical integrity. HIOs can be maintained as long-term cultures for periods longer than a year, but this requires periodically cutting open mature spheres into individual pieces,[25] which then reform into intact, closed, spherical organoids.[15,16] Thus, methods for establishing control over luminal and extraluminal transport are clearly needed.

A common approach for establishing well-defined flow control within a tissue culture is to integrate the tissue into a microfluidic or millifluidic device.[26–28] This typically involves directing microscale fluid flow together with engineered cell scaffolds to replicate the structure and function of a specific human tissue or organ. For example, human "organ-on-a-chip" systems that are designed to replicate the kidney,[29–32] heart,[33–38] lung,[39–45] intestine,[40,46–52] liver,[44,47,51,53–64] blood vessels,[42,43,65–67] bone,[68–70] marrow,[71] nerve,[72–77] muscle[78] and cornea[79] have been developed. The exquisite control of liquid flow provided by fluidic devices can be used to deliver minute quantities of chemical or biological material with spatial and temporal precision,[27,28] allows for on-demand monitoring and analysis of nanoliter and picoliter liquid volumes,[26] and can be used to maintain chemostasis.[28]

Most organ-on-chip systems use traditional cell cultures. By contrast, the integration of organoid cultures into fluidic systems has been limited. In one approach, cells from

disrupted human gastrointestinal organoids have been templated with microfluidic channels:[80,81] a promising method that controls organoid structure and provides access to the luminal space. In another approach, preformed organoids including liver, cardiac, and vascular organoids were combined into a single, circulatory microfluidic system to create a "body-on-a-chip" platform.[82,83] The use of intact, preformed organoids precludes the use of artificial scaffolding and allows the tissue culture to form in an environment more representative of *in vitro* conditions before integration into the chip; however, for gastrointestinal organoids, access to the luminal space remains challenging. Short-term luminal flow has been established through human gastric organoids (HGOs),[19] but the time scale of flow has been limited, and the impact of luminal flow on organoid viability is not clear. A fluidic device capable of establishing long-term flow through gastrointestinal organoids is still needed.

Results and discussion

To demonstrate the transport limitations caused by the closed epithelial shell, we follow the accumulation of waste inside the lumen of an HIO over several days using time-lapse light microscopy. Our imaging reveals that colloidal-scale cell debris sloughs off from the inner surface of the HIO and settles to the bottom of the lumen where it remains for multiple days (image series, Fig. 1A and B and Video S1†). As waste builds, HIOs eventually darken and become optically opaque, as shown by the image in Fig. 1C. While the images in Fig. 1 provide a visual depiction of waste accumulation, dissolved molecular-scale waste, and metabolites which are not visible also likely accumulate due to the semipermeable nature of the epithelial shell.[13,15–17,24] Accumulation of waste impacts organoid viability and physiology and limits the time period over which organoids remain viable for experimentation.[13]

To establish real-time control over luminal contents, we develop a chip-based fluidic device for establishing luminal liquid flow. Mature HIOs are millimeters in diameter; so, a fabrication method capable of generating a device with millimeter-scale features and channels is needed. To achieve device features at this scale, we use a laser to cut thin acrylic sheets into precise shapes. Our device consists of three layers: a middle layer containing the organoid and a channel for extraluminal flow, and an upper and lower layer which enclose the middle layer (Fig. 2A). These layers are then sandwiched together to form a three-dimensional millifluidic device (Fig. 2B). Thin, laser-cut silicone rubber sheets are also included between acrylic layers to seal the device and prevent leaking. Holes in the upper acrylic layer allow for the introduction of liquid into and out of the upper (extraluminal) flow channel, and the bottom layer forms the floor of the device. Laser-cut cylindrical side channels with long axes normal to the side walls of the device and perpendicular to the layer plane (Fig. 2C) allow for tapered glass capillaries to be inserted into the HIO. Luminal
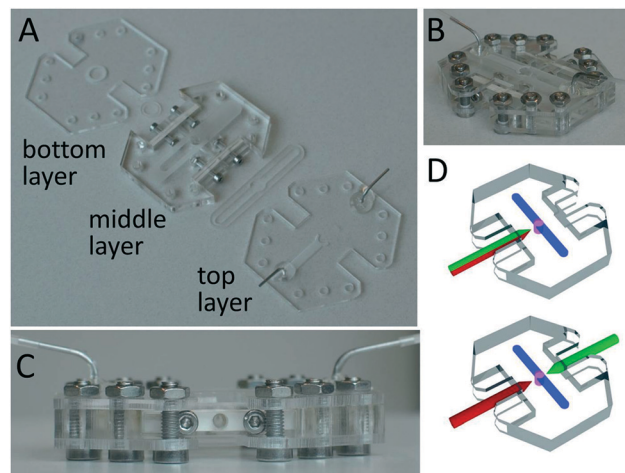

Fig. 2 Multilayer millifluidic chip for establishing distinct luminal and extraluminal flow. (A) The device is composed of three layers. The HIO is contained in a central well in the middle layer. Extraluminal flow is guided by an engraved channel in the top layer just above the organoid. The bottom layer encloses the bottom of the device. Arrows indicate laser-cut silicone gaskets. (B) Orthogonal view of the assembled device with fluidics assembled for extraluminal flow but no capillaries yet inserted for HIO porting. (C) Side view of the assembled device with the side port gasket (white) clearly visible. (D) Illustrations highlighting two different configurations for HIO porting. Upper: Porting with a single, double-lumen capillary (green-red). Lower: Porting with two, single-lumen capillaries (red and green).

flow is established in one of two ways: using a single double-lumen capillary (Fig. 2D, bottom) or two single-lumen capillaries (Fig. 2D, top). Laser-cut silicone rubber gaskets are used on the sides as compression seals to prevent leakage. The modular design of the device allows each layer to be designed independently and the device to be disassembled and reassembled for sterilization and repeated use. The transparency of the acrylic allows for optical imaging of a ported HIO.

To establish flow through an organoid, the lower and middle layers (Fig. 2A) are assembled under sterile conditions. An HIO embedded in Matrigel is then placed in the circular well formed by the two layers, and the organoid is punctured on one or two sides by manipulating tapered capillaries using independent three-axis micromanipulators. An HIO before and after puncturing is depicted in Fig. 3A and B, respectively. Most organoids, when punctured,
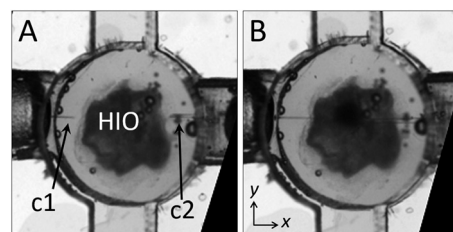

Fig. 3 HIO porting process. (A) Microscopy image of HIO in an assembled device before puncturing with capillaries (c1, c2). (B) Image of the same HIO after puncturing on either side. The diameter of the circular well in (A) and (B) is 4 mm.

deflate slightly but do not immediately collapse. This is due to the fact that the outer surface of the organoid attaches to the surrounding Matrigel through cellular adhesions. Matrigel is viscoelastic with a characteristic relaxation time on the order of tens of minutes, which provides sufficient time to puncture both sides and establish flow. We find that HIOs with diameters between 2 mm and 3 mm are ideal for porting in our device; HIOs with diameters larger than 3 mm typically have a large amount of accumulated waste, which leads to clogging of the outlet capillary, and organoids with diameters smaller than 1 mm are difficult to manipulate with our current setup. While this lower size limit precludes the use of mouse organoids and human organoids derived from primary tissues, which are an order of magnitude smaller in diameter than HIOs derived from iPSCs,[18,25] a smaller version of a GOFlowChip imaged with appropriate optics could be used to port organoids and spheroids with sub-mm scale sizes. After the HIO is punctured, the upper layer is added to the assembly, and the device is sealed by compression. To drive luminal liquid flow through the HIO, the outer ends of the glass capillaries are attached through microfluidic tubing to computer-controlled syringe pumps, two of which provide independent control over the infusion and withdrawal of liquid from the organoid. To drive liquid flow through the extraluminal flow channel, ferrules inserted into the top layer of the chip (Fig. 2A–C) are connected through microfluidic tubing to other computer-controlled syringe pumps. A detailed description of the loading and assembly protocol, including the most commonly encountered problems, is included in ESI† along with the design files needed to fabricate the device.

A ported HIO will ideally possess the same barrier integrity found in the native gastrointestinal tract. In an unported HIO, barrier integrity is maintained by the epithelial shell *via* intact cellular tight junctions; however, when the shell is punctured, integrity is contingent on the formation of a seal at the puncture site. To test the seal of a fully ported HIO, we pressurize the HIO by flowing liquid through the left-side capillary, c1 (q_{in} = 5 μL h^{-1}) while suppressing liquid outflow through the right-side capillary, c2 (q_{out} = 0). Thus, a seal forms at the puncture site which allows for dramatic inflation without any leakage of liquid even over several hours, as shown by the series of images in Fig. 4A (Video S2†). High-resolution imaging suggests that Matrigel plays a role in maintaining this seal by closing around the capillary until the ruptured epithelium regrows and adheres to the capillary. This is not surprising, given that gut organoids are commonly punctured, injected with material, and the capillary removed without observable deflation or ejection of luminal contents.[12] We note that the temporary barrier provided by Matrigel differs from that provided by intact epithelium; while Matrigel suppresses liquid flow and the diffusion of colloidal-scale objects,[84] molecules smaller than the mesh size of the gel ($\xi \approx$ 10 nm) diffuse through the gel.[85] Thus, for experiments where barrier integrity immediately following HIO puncture is
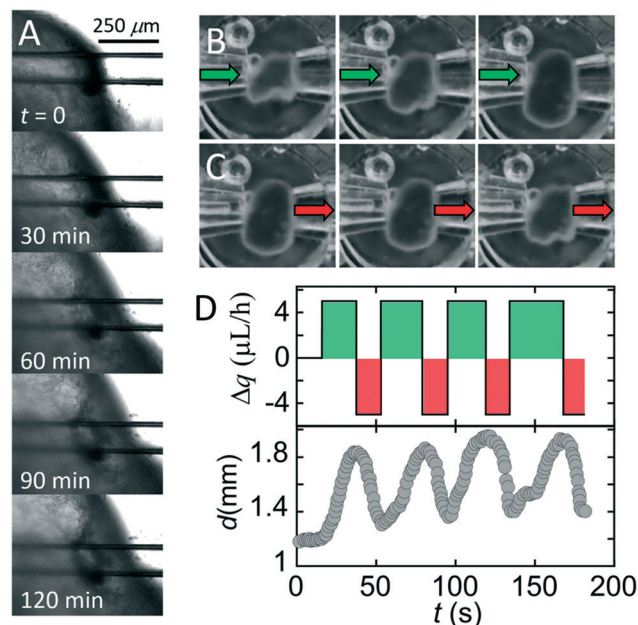

Fig. 4 Demonstration of puncture seal and luminal flow. (A) Microscopy image series. An HIO punctured on both sides and subjected to a net influx of liquid (q_{in} = 5 μL h^{-1}; q_{out} = 0 μL h^{-1}) swells, but no leaking of liquid at the puncture site is detected. (B) Microscopy image series. An HIO punctured on both sides swells as aqueous media is infused from the left capillary (q_{in} = 5 μL h^{-1}). No liquid is removed from the HIO through the right capillary (q_{out} = 0 μL h^{-1}). Time between images is 20 s. (C) Microscopy image series. The HIO shrinks as media is withdrawn through the right capillary (q_{out} = 5 μL h^{-1}; q_{in} = 0 μL h^{-1}). Images in each series (B and C) are separated by Δt = 20 s. (D) Upper plot. Net flow of media, $\Delta q = q_{in} - q_{out}$, into or out of the HIO is plotted as a function of time. Lower plot. Corresponding change in HIO diameter, d (y-axis) as a function of time in response to infusion and withdrawal.

critical, the nature of the seal and time needed to ensure complete epithelium healing should be investigated further. To establish luminal flow and verify the integrity of the ported seal, we design a flow sequence that should result in organoid inflation and deflation. The inflation condition is achieved by infusing liquid media through c1, while preventing flow through c2, resulting in a positive net flow of media into the organoid, Δq. Here, $\Delta q = q_{in} - q_{out}$, where q_{in} is the total flow rate into the organoid and q_{out} is the total flow rate out of the organoid. The deflation condition is achieved by withdrawing liquid from c2, while preventing flow through c1, resulting in a negative net flow of liquid (q_{in} < q_{out}). We initiate this flow sequence, alternating between the two flow conditions, and observe that the organoid undergoes striking volume changes in response to flow, as depicted by the series of images in Fig. 4B and C (Video S3†). To quantify this volume change, we plot the net imposed flow rate as a function of time (Fig. 4D, top plot) along with the maximum diameter of the organoid measured along the y-axis as a function of time (Fig. 4D, bottom plot), and observe that the diameter changes consistently in response to the imposed flow. This represents, to our knowledge, the first

demonstration of luminal flow through a topologically closed gastrointestinal organoid.

For long-term experimentation, the chip must be capable of maintaining luminal flow through an HIO for hours and even days. In preliminary attempts, we find that establishing flow for this length of time is limited mainly by clogging of the exit capillary. Clogging presents a problem because syringe pumps are flow rate-controlled rather than pressure-controlled and thus insensitive to pressure buildup in the HIO; if blockage of the exit capillary occurs, liquid is driven into the HIO until it ruptures. To mitigate this, we explore a range of exit tip diameters (20 μm ≤ d ≤ 120 μm) and find that for fully differentiated organoids containing a significant amount of waste, an exit capillary with a tip diameter $d \approx 80$ μm and a flow rate $q_{out} \leq 5$ μL h^{-1} is ideal; capillaries with smaller tip diameters tend to clog, and capillaries with larger tip diameters are difficult to puncture HIOs. We also find that during long-term experiments bubbles form in the overflow liquid, which negatively impacts image quality and HIO barrier integrity. Thus, to suppress bubble formation, we pressurize the liquid slightly by constricting the outlet of the overflow liquid (see Experimental). After significant optimization we regularly establish steady-state flow through HIOs for $t \geq 65$ h using both the single, double-lumen capillary and double, single-lumen capillary porting methods

(Videos S4 and S5†); longer flow experiments could be achieved but we were limited by microscope access in our shared facility. Luminal flow on the order of days will enable a wide variety of future experiments.

A continuous luminal flow could be used to introduce materials to the lumen or remove and sample luminal contents. To demonstrate the value of luminal flow, we port an HIO containing significant accumulated waste and use flow to remove waste. The HIO is ported using capillaries with tip diameters c1 = 40 μm and c2 = 80 μm, steady state flow is established by setting flow into and out of organoid equal ($q_{in} = q_{out} = 5$ μL h^{-1}), and the organoid is imaged for 20 h. During this time, the organoid undergoes significant fluctuations, moving in and out of our objective focus (Video S6†); however, no leaking, signs of cell death, or loss of barrier integrity are observed. At the 20 h mark, when the microscope is refocused, it is apparent that the HIO has clarified, and that waste is being removed by liquid flow through the exit capillary (Fig. 5A). The organoid continues to clarify over the next 7 hours as depicted by the series of microscopy images in Fig. 5B–D. Waste is observed exiting the organoid through c2. Images of the flow profile along c2 reveal the movement of large objects moving from left to right as they are carried by liquid flow, as shown by the series of microscopy images in Fig. 5E (Video S7†). To determine the velocity of waste exiting the HIO, we measure the intensity profile along the center of the capillary as a function of time and plot the data as a kymograph in Fig. 5F. In this format, the y-axis represents the grayscale pixel intensity along a horizontal line bisecting the images in Fig. 5E, and the x-axis represents time. Thus, the lines moving from the bottom left to the upper right represent the movement of objects from left to right within c2, and the slope of these lines provides their velocity. The dark line represents the large piece of waste depicted by the image series in Fig. 5E with a velocity, $v = 27$ μm s^{-1}. The green crosses in Fig. 5E represent the positions associated with the pixels marked by the green crosses in Fig. 5F. This result demonstrates qualitatively that luminal flow can be used to perform a useful function: the removal of accumulated waste.

Ideally, flow through a ported HIO will mimic flow through the human gut. The topology of a dual-ported HIO, with an inlet and outlet on opposing sides, is identical to that of the gut, but the dimensions and aspect ratio differ significantly. A dual-ported HIO is a short tube with equal diameter and length ($d \approx 3–5$ mm); by comparison, the lumen of the human intestine is an order of magnitude wider in diameter ($d \approx 2–3$ cm), and the length of the human intestine is three orders of magnitude longer ($\ell \approx 2–3$ m) than an HIO. Because of these differences in size and aspect ratio, matching the volumetric flow rate would result in flow conditions that are unrealistically fast, which could result in the removal of not just waste, but also key molecules that are critical to epithelial health and function. Instead of flow rate, liquid velocity, v appears to be the relevant parameter as it controls the rate at which materials are transported to and
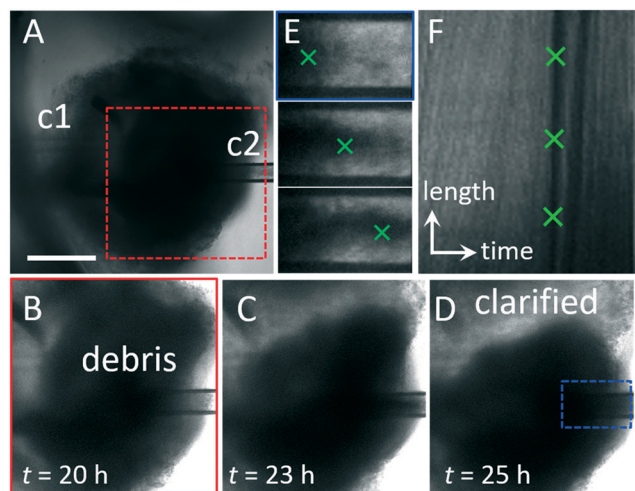

Fig. 5 Clearing waste with luminal flow. (A) Microscopy image series. Steady state luminal flow is established in an HIO with significant waste accumulation by setting $q_{in} = q_{out} = 5$ μL h^{-1}. Flow is from left to right. After 20 h, the HIO is still viable, and no blebbing or leaking is observed. (B–D) Over time, the HIO becomes more transparent as waste is carried by liquid flow through c2. Images correspond to region in (A), red dashed box. The clarified region of the lumen is labeled in (D). (E) Series of images of c2 depict movement of the waste exiting the organoid from left to right. Images correspond to region in (D), blue dashed box. (F) Kymograph representing the intensity profile along a line in the center of the channel in c2 (E) is plotted (y-axis) as a function of time (x-axis). The dark line indicated by the green crosses represents a large piece of waste moving from left to right along the channel. The scale of the y-axis represents 150 μm and the scale of the x-axis represents 150 minutes. The slope of the line represents the velocity, $v = 27$ μm s^{-1}.

from the inner wall of the epithelium, as well as determining the stress exerted by the luminal contents on the inner lining of the gut, which is critical for gut physiology. The average velocity through the human gut is reported to be on the order of 0.4 mm s^{-1}.[86,87] For comparison, the average velocity in our pulsatile experiment (Fig. 3), where q = 25 μL min^{-1}, d = $2r \approx 1.5$ mm, is $v = q/\pi r^2 \approx 0.24$ mm s^{-1}. Thus, the luminal flow velocity through our HIOs is comparable to that in the human gut. We note that the shear stress exerted by luminal contents on the inner wall of the gut is also governed by the topography of the gut lining and the rheological properties of the material in the lumen, and the impact of these parameters on HIO physiology warrant further investigation.

Similarly, flow outside a ported HIO should ideally mimic flow around the outside of the human gut. To determine the relevant range for extraluminal flow in our HIO chip, we begin by considering the frequency of media exchange needed to maintain HIOs under standard culture conditions. Cultured HIOs require media replacements of 50 μl per HIO every 48 h, which is approximately equal to 1 μl h^{-1} of continuous flow in our chip for a single HIO. In the native human gut, the transport of blood through gut tissue is on the order of 10 μl h^{-1} mg^{-1} of tissue, which corresponds to continuous flow on the order of 10 s of μl h^{-1} in our chip for a single HIO (see Experimental). For practical purposes, in the experiments described here we use flow rates in the range 50 μl h$^{-1} \leq q \leq 300$ μl h^{-1}, but to explore the impact of extraluminal flow on HIO physiology, q could be significantly reduced. In the future, additional changes could be made to mimic physiologically relevant conditions. For example, media composition could be altered such that oxygen-poor, nutrient-rich liquid is delivered to the lumen and oxygen-rich, nutrient-poor liquid is delivered to the basolateral surface. Additionally, the structure of the material around the HIO could be engineered to mimic the complex, layered tissues around the native gut, which govern liquid flow and transport and contain vasculature.

To determine if puncturing the epithelium and subjecting HIOs to long-term luminal and extraluminal flow adversely affects HIO viability, we perform measurements of cell viability using flow cytometry. Ported HIOs subjected to flow for t = 65 h are removed from the device, individually dispersed as single cell suspensions, stained with a fluorescent indicator of membrane integrity (intracellular/extracellular amines stained with a Live/Dead cell stain, ThermoFisher Inc.) that differentially labels viable and nonviable cells, and assayed using flow cytometry (see Experimental). A histogram of stain fluorescence intensity reveals a bimodal distribution (Fig. 6A), representing the fraction of live and dead cells from each HIO. When the data are compared (Fig. 6C), we find that the fraction of dead cells in ported HIOs (mean ± SD: 0.1296 ± 0.063, n = 3) was not statistically different from our two controls: unported HIOs assayed individually (0.1555 ± 0.1115, n = 4) and unported HIOs combined and assayed together (0.177 ± 0.0512, n = 3) (ANOVA: $F_{2,7}$ 0.64, P = 0.55). This critical
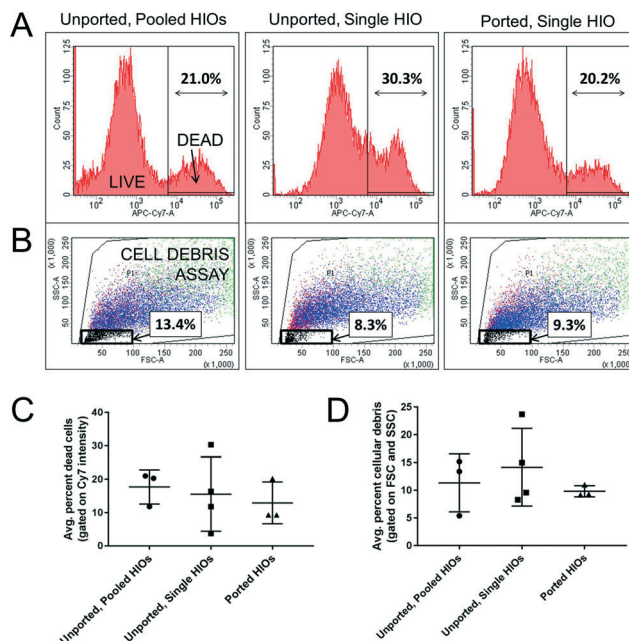

Fig. 6 Flow cytometry results show that HIO viability is not adversely affected by porting and luminal flow. (A) Representative flow cytometry histograms of near-IR fluorescence intensity (APC-Cy7-A) from homogenized HIOs reveal two populations of cells: live (low intensity) and dead (high intensity). (B) Forward (FSC) and side (SSC) scattering at low intensities provide a measure of cellular debris as indicated by the black box and percentage values. (C) The average percent of dead cells present in HIOs that were either unported or ported, as determined by the LIVE/DEAD cell staining data represented in (A). (D) The average percent of cell debris present in HIOs that were either unported or ported, as determined by the scattering data represented in (A).

experiment and positive result support our microscopy observations that HIO viability is not adversely affected by porting and luminal flow. In the future, the impact of flow velocity, luminal content rheology, and nutrient concentration on gene expression, cellular differentiation, and cellular proliferation should be investigated to determine how these parameters impact the distribution of cell types and behaviors in an HIO.

Flow cytometry can also provide a measure of insoluble cellular debris; particles with low intensity forward and side scattering are characteristic of suspended particles with sizes smaller than a cell (Fig. 6B). When these data are compared (Fig. 6D), we also find that the fraction of scattering events in ported HIOs corresponding to cellular debris (mean ± SD: 0.098 ± 0.01, n = 3) was not statistically different from controls: unported HIOs assayed individually (0.1415 ± 0.07, n = 4) and unported HIOs assayed collectively (0.1133 ± 0.0522, n = 3) (ANOVA: $F_{2,7}$ = 1.42, P = 0.30). While this is somewhat surprising given the dramatic removal of luminal waste depicted in Fig. 5, it could be that luminal HIO waste is solubilized during preparation for flow cytometry and no longer scatters light. It is also possible that even though more debris is being removed, the epithelium is producing more waste because it is more active in the ported state.

Regardless, it is clearly apparent from microscopy that luminal material is being removed by the porting and flow process in manner which is physiologically relevant. In the future, more specific chemical or biochemical assays for quantifying the luminal concentrations of specific metabolic byproducts and waste as a function of luminal flow should be explored.

We expect that the results presented here will enable a wide variety of experiments. Luminal flow provides a means of introducing materials to the luminal space as well as extracting materials from this space; so, the device will be ideal for experiments exploring the establishment and stability of the microbiome, including the introduction of microbes, monitoring microbial dynamics with fluorescence microscopy, and detecting the presence of detached microbes and dissolved waste products and metabolites in the luminal effluent. In addition, maintained barrier integrity and independent control of luminal and extraluminal liquid streams will allow researchers to explore the transport of substances across the epithelial shell. For example, the absorption of nutrients and pharmaceutical compounds from the lumen through the apical surface of the epithelium could be explored. Inversely, the excretion of materials such as mucus and fluid into the lumen could also be studied. The functionality of the millifluidic chip presented here could be enhanced through the integration of a variety of soft, PDMS-based microfluidic modules such as flow-focusing drop makers and detection and sorting capabilities.[88,89] While the design presented here could be parallelized to port small numbers of HIOs, the delicate porting process is not amenable to high-throughput testing. Truly massive parallelization would require the development of an automated porting method as well as improvements in HIO culture techniques to generate large numbers of HIOs with monodisperse sizes.

Conclusions

In conclusion, the gut organoid flow chip (GOFlowChip), presented here represents the first device engineered to establish liquid flow through the lumen of a gastrointestinal organoid for multiple days. This is achieved by pressurizing the device to suppress bubble formation and optimizing device design to prevent clogging. While the limits of HIO culturing and experimentation have not been fully explored, this prototype provides a significant advancement by mimicking a critically important physiologic parameter of the human gut: long-term luminal flow. Moreover, the chip holds several other advantages over previous gut organoid chip designs: the multilayer design allows for straightforward assembly, disassembly, sterilization, and reuse; a seal which forms at each epithelial puncture site allows for independent control of luminal and extraluminal liquid flow conditions, and biological assays of cell viability confirm the long-term viability of HIOs in the device. Thus, the GOFlowChip opens

the field for broader application of HIO models in biomedical research.

Experimental

Device fabrication

Multilayer devices composed of three distinct layers and silicone rubber gaskets were cut from clear cast acrylic plastic sheets (McMaster Carr; dimensions: 12″ × 12″) and silicone rubber sheets (McMaster Carr, Durometer 40A, White; dimensions: 12″ × 12″, 1/16″ thickness) using an automated laser cutter (Universal). Top and bottom layers were cut from sheets with thicknesses of $h = 2.0$ mm and $h = 1.5$ mm, respectively. The middle layer was cut from $h = 4.5$ mm thick sheets. Layers and gaskets were designed using AutoCAD software and design files are included in the ESI† section. Layers were sealed through gaskets between each layer and compressing the assembled layers using nuts and bolts (McMaster Carr; 316 stainless steel, M3 × 0.3 mm thread, 10 mm length). For the single-lumen, two capillary setup; tapered glass capillaries for puncturing the HIOs were created by pulling thin-wall borosilicate glass capillaries (World Precision Instruments TW150-6) using a micropipette puller (Sutter Instruments, P-97). Capillaries with tip diameters between 40 μm and 80 μm and taper lengths of 4 mm and 3.5 cm were used. For dual-lumen, single capillary setup; septum theta borosilicate glass capillaries (World Precision Instruments TST150-6) were pulled in the same way to obtain a 100 μm tip with 3 mm taper length. Capillaries were mounted to three-axis translational micromanipulators (Quater Research; XYZ 300 ML) with capillary holders designed in Fusion 360 and 3D printed using SLA 3D printer (see design files) for precision control during organoid puncturing.

Liquid flow

Luminal and extraluminal liquids were introduced to the device by connecting liquid-filled syringes (Hamilton 500 μL and BD 10 mL, respectively) fitted with blunt-tip stainless steel dispensing needles (McMaster Carr; luminal flow: 26 gauge and 17; extraluminal flow: 16 gauge) to medical grade polyethylene micro-tubing (Scientific Commodities Inc., PE/9, ID = 1.40 mm, OD = 1.91 mm). For luminal flow, tubing was connected to the non-tapered ends of the glass capillaries. For extraluminal flow, tubing was connected to blunt-tip stainless steel dispensing needles (McMaster Carr, 90° angle, 20 gauge) inserted into holes in the upper layer of the device. Both luminal and extraluminal liquid flow was driven by programmable, computer-controlled New Era NE-1000 syringe pumps for precise delivery and withdrawal of small volumes of liquid. For short-term periodic flow experiments, phosphate-buffered saline (PBS) was used for both luminal and extraluminal flow. For long-term, steady-state flow experiments, HIO growth media was used for both luminal and extraluminal flow. To establish a

baseline for extraluminal flow, we estimate the transport of blood through gut tissue in the native human gut.

We estimate cardiac output to be 5 L min^{-1} of which 20% is shared between the spleen, liver, stomach, small intestine and large intestine which are approximately 5 kg in total.[90–93] This corresponds to approximately 10 μl h^{-1} mg^{-1} of tissue. The HIOs used in our experiments contain tissue mass on the order of 2–5 mg, so we estimate the baseline for extraluminal flow to be 20–50 μl h^{-1}.

Sterilization

The glass transition of the cast acrylic sheets is below our autoclave temperature range ($T \approx$ 121–132 C), so sterilizing the millifluidic device using heat is not feasible. Instead, the device was sterilized by disassembling individual layers and soaking them in pure ethanol for five minutes, followed by rinsing in autoclaved distilled water. After assembly, the device and associated tubing and connectors were again flushed with pure ethanol followed by autoclaved distilled water.

Bubble suppression

The pressure required to drive liquid flow through a microfluidic device is usually sufficient to suppress air bubble formation in the device; however, this is not the case for millifluidic devices. To suppress bubble formation, we pressurized the liquid by attaching a tapered capillary at the outlet of the overflow channel. We observed that flow rates of 100–150 μl h and exit tip diameters of 40–60 μm corresponding to pressure drops of 70–140 Pa were sufficient to suppress bubble formation during multiday flow experiments.

Imaging

Time-lapse video microscopy measurements were performed using a laser scanning confocal microscope (Leica SP5 II) equipped with an environmental control chamber (Life Imaging Services) maintained at 37 °C. Fluorescence and brightfield images were collected with 10× air objective (Leica 506 505, HC PL Fluotar 10×/0.03) and 1.25× air objective (Leica 506 215, HCX PL Fluotar 1.25×/0.04). Time-lapse measurements were also collected using a stereomicroscope (Leica, M205 FA) equipped with color CMOS video camera (Leica, DFC3000 G). After collection, images were processed and analyzed using IMARIS, MetaMorph and ImageJ image analysis software.

Organoid culture

Derivation and maintenance of HIOs followed published protocols.[1,25] Briefly, HIOs were embedded in Matrigel (BD Biosciences) and overlaid with Advanced DMEM-F12 medium (Invitrogen, Carlsbad, CA) containing 1× B27 supplement (Invitrogen), 1× GlutaMAX (Life Technologies, Carlsbad, CA), 10 μM Hepes, 10% pen/strep, 100 ng mL^{-1} rhNoggin (R&D

Systems), 100 ng mL^{-1} epidermal growth factor (R&D Systems), and approximately 500 ng mL^{-1} R-Spondin1 (RSPO1). RSPO1 was obtained from conditioned media collected from a HEK293 cell line that was stably transfected and zeocin-selected for the RSPO1 expression vector. Media was changed every two to four days, and HIOs were transferred to fresh Matrigel once a week until they reached approximately 2 to 3 mm in diameter for experiments. This size was reached on average 48 days after initial spheroid formation.

Cell viability and cellular debris assays

Cell viability and cellular debris assays were determined using a LIVE/DEAD Fixable Dead Cell Stain Kit (ThermoFisher) and flow cytometry. Ported HIOs were collected after being subjected to luminal flow for $t \geq 65$ h and preparation of the HIOs for the LIVE/DEAD stain occurred within 1 hour of collection. To disperse HIOs as single-cell suspensions, individual HIOs were washed with PBS, incubated in 0.25% trypsin–EDTA, and subjected to mechanical shear by passing the HIO through a P1000 pipette tip or 21 gauge needle. Cells were then washed in PBS, incubated with fluorescent dye, and fixed with formaldehyde following the manufacturer's instructions. Cell viability, as determined by near-IR fluorescence intensity, was quantified using a LSRFortessa flow cytometer, fluorescence-activated cell sorting (FACS), and FACSDiva software (BD Biosciences). Gating single cells was based on forward and side-scatter profiles using an isotype control made from a pooled sample of four unported HIOs that were maintained under static cell culture conditions. The percentages of live and dead cells were determined by using the manufacturer's recommended settings and guidelines. After removing doublets and cell clumps from analysis, infrared staining was analyzed to determine the best fit of separation between live cells and dead cells, which are represented by low and high APC-Cy7-A emission intensity, respectively. As an additional control, unported HIOs similar in size and age to the ported HIOs were collected and analyzed individually following the protocol above.

Statistical analysis

A one-way ANOVA with multiple comparisons was performed to test statistical differences between the means of three groups: unported, pooled HIOs; unported, single HIOs; and ported HIOs.

Author contributions

Conceptualization: S. T. W., J. N. W., and J. R. S.; methodology: S. T. W., J. N. W., J. R. S., B. S., and B. R. J.; investigation: B. S., B. R. J., and S. H.; writing – original draft: J. N. W., S. T. W., B. S., and B. R. J.; writing – review & editing: J. N. W., S. T. W., B. S., J. R. S., and B. R. J.; funding acquisition: S. T. W., J. R. S., and J. N. W.; resources: S. T. W.,

J. R. S., and J. N. W.; supervision: S. T. W., J. R. S., and J. N. W.

Funding

Conflicts of interest

There are no conflicts to declare.

Notes and references

1 J. R. Spence, C. N. Mayhew, S. A. Rankin, M. F. Kuhar, J. E. Vallance, K. Tolle, E. E. Hoskins, V. V. Kalinichenko, S. I. Wells, A. M. Zorn, N. F. Shroyer and J. M. Wells, *Nature*, 2011, **470**, 105–109.

2 T. Sato, D. E. Stange, M. Ferrante, R. G. J. Vries, J. H. van Es, S. van den Brink, W. J. van Houdt, A. Pronk, J. van Gorp, P. D. Siersema and H. Clevers, *Gastroenterology*, 2011, **141**, 1762–1772.

3 D. R. Hill, S. Huang, M. S. Nagy, V. K. Yadagiri, C. Fields, D. Mukherjee, B. Bons, P. H. Dedhia, A. M. Chin, Y. H. Tsai, S. Thodla, T. M. Schmidt, S. Walk, V. B. Young and J. R. Spence, *eLife*, 2017, **6**, e29132.

4 S. R. Finkbeiner, X. L. Zeng, B. Utama, R. L. Atmar, N. F. Shroyer and M. K. Estes, *mBio*, 2012, **3**, e00159-12.

5 C. A. Lindemans, M. Calafiore, A. M. Mertelsmann, M. H. O'Connor, J. A. Dudakov, R. R. Jenq, E. Velardi, L. F. Young, O. M. Smith, G. Lawrence, J. A. Ivanov, Y. Y. Fu, S. Takashima, G. Q. Hua, M. L. Martin, K. P. O'Rourke, Y. H. Lo, M. Mokry, M. Romera-Hernandez, T. Cupedo, L. E. Dow, E. E. Nieuwenhuis, N. F. Shroyer, C. Liu, R. Kolesnick, M. R. M. van den Brink and A. M. Hanash, *Nature*, 2015, **528**, 560–564.

6 K. Nozaki, W. Mochizuki, Y. Matsumoto, T. Matsumoto, M. Fukuda, T. Mizutani, M. Watanabe and T. Nakamura, *J. Gastroenterol.*, 2016, **51**, 206–213.

7 J. M. Wells and J. R. Spence, *Development*, 2014, **141**, 752–760.

8 M. Aurora and J. R. Spence, *Dev. Biol.*, 2016, **420**, 230–238.

9 P. H. Dedhia, N. Bertaux-Skeirik, Y. Zavros and J. R. Spence, *Gastroenterology*, 2016, **150**, 1098–1112.

10 J. L. Forbester, D. Goulding, L. Vallier, N. Hannan, C. Hale, D. Pickard, S. Mukhopadhyay and G. Dougan, *Infect. Immun.*, 2015, **83**, 2926–2934.

11 J. L. Leslie, S. Huang, J. S. Opp, M. S. Nagy, M. Kobayashi, V. B. Young and J. R. Spence, *Infect. Immun.*, 2015, **83**, 138–145.

12 M. A. Engevik, M. B. Yacyshyn, K. A. Engevik, J. Wang, B. Darien, D. J. Hassett, B. R. Yacyshyn and R. T. Worrell, *Am. J. Physiol.*, 2015, **308**, G510–G524.

13 K. L. Sinagoga and J. M. Wells, *EMBO J.*, 2015, **34**, 1149–1163.

14 S. R. Finkbeiner, D. R. Hill, C. H. Altheim, P. H. Dedhia, M. J. Taylor, Y.-H. Tsai, A. M. Chin, M. M. Mahe, C. L. Watson, J. J. Freeman, R. Nattiv, M. Thomson, O. D. Klein, N. F. Shroyer, M. A. Helmrath, D. H. Teitelbaum, P. J. Dempsey and J. R. Spence, *Stem Cell Rep.*, 2015, **4**, 1140–1155.

15 A. Buckley and J. R. Turner, *Cold Spring Harbor Perspect. Biol.*, 2018, **10**, a029314.

16 D. R. Hill, S. Huang, Y. H. Tsai, J. R. Spence and V. B. Young, *J. Visualized Exp.*, 2017, **130**, e56960.

17 H. Gray and S. Standring, *Gray's anatomy: the anatomical basis of clinical practice*, Churchill Livingstone, 2008.

18 T. A. Sebrell, B. Sidar, R. Bruns, R. A. Wilkinson, B. Wiedenheft, P. J. Taylor, B. A. Perrino, L. C. Samuelson, J. N. Wilking and D. Bimczok, *Cell Tissue Res.*, 2018, **371**, 293–307.

19 K. K. Lee, H. A. McCauley, T. R. Broda, M. J. Kofron, J. M. Wells and C. I. Hong, *Lab Chip*, 2018, **18**, 3079–3085.

20 X. L. Yin, B. E. Mead, H. Safaee, R. Langer, J. M. Karp and O. Levy, *Cell Stem Cell*, 2016, **18**, 25–38.

21 R. Cruz-Acuña, M. Quirós, A. E. Farkas, P. H. Dedhia, S. Huang, D. Siuda, V. García-Hernández, A. J. Miller, J. R. Spence, A. Nusrat and A. J. García, *Nat. Cell Biol.*, 2017, **19**, 1326.

22 R. Cruz-Acuña, M. Quirós, S. Huang, D. Siuda, J. R. Spence, A. Nusrat and A. J. García, *Nat. Protoc.*, 2018, **13**, 2102–2119.

23 M. M. Capeling, M. Czerwinski, S. Huang, Y.-H. Tsai, A. Wu, M. S. Nagy, B. Juliar, N. Sundaram, Y. Song, W. M. Han, S. Takayama, E. Alsberg, A. J. Garcia, M. Helmrath, A. J. Putnam and J. R. Spence, *Stem Cell Rep.*, 2019, **12**, 381–394.

24 N. C. Zachos, O. Kovbasnjuk, J. Foulke-Abel, J. In, S. E. Blutt, H. R. de Jonge, M. K. Estes and M. Donowitz, *J. Biol. Chem.*, 2016, **291**, 3759–3766.

25 K. W. McCracken, J. C. Howell, J. M. Wells and J. R. Spence, *Nat. Protoc.*, 2011, **6**, 1920–1928.

26 A. J. deMello, *Nature*, 2006, **442**, 394–402.

27 J. El-Ali, P. K. Sorger and K. F. Jensen, *Nature*, 2006, **442**, 403–411.

28 I. Maschmeyer, A. K. Lorenz, K. Schimek, T. Hasenberg, A. P. Ramme, J. Hubner, M. Lindner, C. Drewell, S. Bauer, A. Thomas, N. S. Sambo, F. Sonntag, R. Lauster and U. Marx, *Lab Chip*, 2015, **15**, 2688–2699.

29 R. Baudoin, L. Griscom, M. Monge, C. Legallais and E. Leclerc, *Biotechnol. Prog.*, 2007, **23**, 1245–1253.

30 K. J. Jang, A. P. Mehr, G. A. Hamilton, L. A. McPartlin, S. Y. Chung, K. Y. Suh and D. E. Ingber, *Integr. Biol.*, 2013, **5**, 1119–1129.

31 K. J. Jang and K. Y. Suh, *Lab Chip*, 2010, **10**, 36–42.

32 L. C. Snouber, F. Letourneur, P. Chafey, C. Broussard, M. Monge, C. Legallais and E. Leclerc, *Biotechnol. Prog.*, 2012, **28**, 474–484.

33 A. Agarwal, J. A. Goss, A. Cho, M. L. McCain and K. K. Parker, *Lab Chip*, 2013, **13**, 3599–3608.

34 W. Cheng, N. Klauke, H. Sedgwick, G. L. Smith and J. M. Cooper, *Lab Chip*, 2006, **6**, 1424–1431.

35 G. A. Giridharan, M. D. Nguyen, R. Estrada, V. Parichehreh, T. Hamid, M. A. Ismahil, S. D. Prabhu and P. Sethu, *Anal. Chem.*, 2010, **82**, 7581–7587.

36 A. Grosberg, P. W. Alford, M. L. McCain and K. K. Parker, *Lab Chip*, 2011, **11**, 4165–4173.

37 G. Khanal, K. Chung, X. Solis-Wever, B. Johnson and D. Pappas, *Analyst*, 2011, **136**, 3519–3526.

38 M. D. Nguyen, J. P. Tinney, F. Ye, A. A. Elnakib, F. P. Yuan, A. El-Baz, P. Sethu, B. B. Keller and G. A. Giridharan, *Anal. Chem.*, 2015, **87**, 2107–2113.

39 C. S. Fritsche, O. Simsch, E. J. Weinberg, B. Orrick, C. Stamm, M. R. Kaazempur-Mofrad, J. T. Borenstein, R. Hetzer and J. P. Vacanti, *Int. J. Artif. Organs*, 2009, **32**, 701–710.

40 O. Y. F. Henry, R. Villenave, M. J. Cronce, W. D. Leineweber, M. A. Benz and D. E. Ingber, *Lab Chip*, 2017, **17**, 2264–2271.

41 D. Huh, H. Fujioka, Y. C. Tung, N. Futai, R. Paine, J. B. Grotberg and S. Takayama, *Proc. Natl. Acad. Sci. U. S. A.*, 2007, **104**, 18886–18891.

42 D. Huh, D. C. Leslie, B. D. Matthews, J. P. Fraser, S. Jurek, G. A. Hamilton, K. S. Thorneloe, M. A. McAlexander and D. E. Ingber, *Sci. Transl. Med.*, 2012, **4**, 159ra147.

43 D. Huh, B. D. Matthews, A. Mammoto, M. Montoya-Zavala, H. Y. Hsin and D. E. Ingber, *Science*, 2010, **328**, 1662–1668.

44 A. Sin, K. C. Chin, M. F. Jamil, Y. Kostov, G. Rao and M. L. Shuler, *Biotechnol. Prog.*, 2004, **20**, 338–345.

45 H. Tavana, P. Zamankhan, P. J. Christensen, J. B. Grotberg and S. Takayama, *Biomed. Microdevices*, 2011, **13**, 731–742.

46 P. Shah, J. V. Fritz, E. Glaab, M. S. Desai, K. Greenhalgh, A. Frachet, M. Niegowska, M. Estes, C. Jäger, C. Seguin-Devaux, F. Zenhausern and P. Wilmes, *Nat. Commun.*, 2016, **7**, 11535.

47 W. L. K. Chen, C. Edington, E. Suter, J. J. Yu, J. J. Velazquez, J. G. Velazquez, M. Shockley, E. M. Large, R. Venkataramanan, D. J. Hughes, C. L. Stokes, D. L. Trumper, R. L. Carrier, M. Cirit, L. G. Griffith and D. A. Lauffenburger, *Biotechnol. Bioeng.*, 2017, **114**, 2648–2659.

48 M. B. Esch, J. H. Sung, J. Yang, C. H. Yu, J. J. Yu, J. C. March and M. L. Shuler, *Biomed. Microdevices*, 2012, **14**, 895–906.

49 H. J. Kim, D. Huh, G. Hamilton and D. E. Ingber, *Lab Chip*, 2012, **12**, 2165–2174.

50 H. J. Kim and D. E. Ingber, *Integr. Biol.*, 2013, **5**, 1130–1140.

51 D. W. Lee, S. K. Ha, I. Choi and J. H. Sung, *Biomed. Microdevices*, 2017, **19**, 37.

52 G. J. Mahler, M. B. Esch, R. P. Glahn and M. L. Shuler, *Biotechnol. Bioeng.*, 2009, **104**, 193–205.

53 J. W. Allen and S. N. Bhatia, *Biotechnol. Bioeng.*, 2003, **82**, 253–262.

54 A. Carraro, W. M. Hsu, K. M. Kulig, W. S. Cheung, M. L. Miller, E. J. Weinberg, E. F. Swart, M. Kaazempur-Mofrad, J. T. Borenstein, J. P. Vacanti and C. Neville, *Biomed. Microdevices*, 2008, **10**, 795–805.

55 P. Chao, T. Maguire, E. Novik, K. C. Cheng and M. L. Yarmush, *Biochem. Pharmacol.*, 2009, **78**, 625–632.

56 S. Cheng, J. M. Prot, E. Leclerc and F. Y. Bois, *BMC Genomics*, 2012, **13**, 54.

57 B. J. Kane, M. J. Zinner, M. L. Yarmush and M. Toner, *Anal. Chem.*, 2006, **78**, 4291–4298.

58 P. J. Lee, P. J. Hung and L. P. Lee, *Biotechnol. Bioeng.*, 2007, **97**, 1340–1346.

59 A. Legendre, R. Baudoin, G. Alberto, P. Paullier, M. Naudot, T. Bricks, J. Brocheton, S. Jacques, J. Cotton and E. Leclerc, *J. Pharm. Sci.*, 2013, **102**, 3264–3276.

60 E. Novik, T. J. Maguire, P. Y. Chao, K. C. Cheng and M. L. Yarmush, *Biochem. Pharmacol.*, 2010, **79**, 1036–1044.

61 A. Sivaraman, J. K. Leach, S. Townsend, T. Iida, B. J. Hogan, D. B. Stolz, R. Fry, L. D. Samson, S. R. Tannenbaum and L. G. Griffith, *Curr. Drug Metab.*, 2005, **6**, 569–591.

62 Y. C. Toh, T. C. Lim, D. Tai, G. F. Xiao, D. van Noort and H. R. Yu, *Lab Chip*, 2009, **9**, 2026–2035.

63 K. Viravaidya and M. L. Shuler, *Biotechnol. Prog.*, 2004, **20**, 590–597.

64 M. B. Esch, J. M. Prot, Y. I. Wang, P. Miller, J. R. Llamas-Vidales, B. A. Naughton, D. R. Applegate and M. L. Shuler, *Lab Chip*, 2015, **15**, 2269–2277.

65 R. Booth and H. Kim, *Lab Chip*, 2012, **12**, 1784–1792.

66 M. C. Liu, H. C. Shih, J. G. Wu, T. W. Weng, C. Y. Wu, J. C. Lu and Y. C. Tung, *Lab Chip*, 2013, **13**, 1743–1753.

67 M. Shin, K. Matsuda, O. Ishii, H. Terai, M. Kaazempur-Mofrad, J. Borenstein, M. Detmar and J. P. Vacanti, *Biomed. Microdevices*, 2004, **6**, 269–278.

68 S. H. Park, W. Y. Sim, B. H. Min, S. S. Yang, A. Khademhosseini and D. L. Kaplan, *PLoS One*, 2012, **7**, e46689.

69 W. T. Zhang, W. Y. Lee, D. S. Siegel, P. Tolias and J. Zilberberg, *Tissue Eng., Part C*, 2014, **20**, 663–670.

70 Y. Zhang, Z. Gazit, G. Pelled, D. Gazit and G. Vunjak-Novakovic, *Integr. Biol.*, 2011, **3**, 39–47.

71 Y. S. Torisawa, C. S. Spina, T. Mammoto, A. Mammoto, J. C. Weaver, T. Tat, J. J. Collins and D. E. Ingber, *Nat. Methods*, 2014, **11**, 183–189.

72 H. S. Park, S. Liu, J. McDonald, N. Thakor and I. H. Yang, *Conf. Proc. IEEE Eng. Med. Biol. Soc.*, 2013, 2833–2835.

73 M. J. Shi, D. Majumdar, Y. D. Gao, B. M. Brewer, C. R. Goodwin, J. A. McLean, D. Lib and D. J. Webb, *Lab Chip*, 2013, **13**, 3008–3021.

74 C. Tsantoulas, C. Farmer, P. Machado, K. Baba, S. B. McMahon and R. Raouf, *PLoS One*, 2013, **8**, e80722.

75 R. van de Wijdeven, O. H. Ramstad, U. S. Bauer, O. Halaas, A. Sandvig and I. Sandvig, *Biomed. Microdevices*, 2018, **20**, 9.

76 R. R. Xiao, W. J. Zeng, Y. T. Li, W. Zou, L. Wang, X. F. Pei, M. Xie and W. H. Huang, *Anal. Chem.*, 2013, **85**, 7842–7850.

77 L. Ziegler, S. Grigoryan, I. H. Yang, N. V. Thakor and R. S. Goldstein, *Stem Cell Rev. Rep.*, 2011, **7**, 394–403.

78 A. Grosberg, A. P. Nesmith, J. A. Goss, M. D. Brigham, M. L. McCain and K. K. Parker, *J. Pharmacol. Toxicol. Methods*, 2012, **65**, 126–135.

79 C. M. Puleo, W. M. Ambrose, T. Takezawa, J. Elisseeff and T. H. Wang, *Lab Chip*, 2009, **9**, 3221–3227.

80 M. Schweinlin, S. Wilhelm, I. Schwedhelm, J. Hansmann, R. Rietscher, C. Jurowich, H. Walles and M. Metzger, *Tissue Eng., Part C*, 2016, **22**, 873–883.

81 M. J. Workman, J. P. Gleeson, E. J. Troisi, H. Q. Estrada, S. J. Kerns, C. D. Hinojosa, G. A. Hamilton, S. R. Targan, C. N.

Svendsen and R. J. Barrett, *Cell. Mol. Gastroenterol. Hepatol.*, 2018, **5**, 669–677.e662.

82 A. Skardal, S. V. Murphy, M. Devarasetty, I. Mead, H. W. Kang, Y. J. Seol, Y. S. Zhang, S. R. Shin, L. Zhao, J. Aleman, A. R. Hall, T. D. Shupe, A. Kleensang, M. R. Dokmeci, S. J. Lee, J. D. Jackson, J. J. Yoo, T. Hartung, A. Khademhosseini, S. Soker, C. E. Bishop and A. Atala, *Sci. Rep.*, 2017, **7**, 8837.

83 Y. S. Zhang, J. Aleman, S. R. Shin, T. Kilic, D. Kim, S. A. M. Shaegh, S. Massa, R. Riahi, S. Chae, N. Hu, H. Avci, W. Zhang, A. Silvestri, A. S. Nezhad, A. Manbohi, F. De Ferrari, A. Polini, G. Calzone, N. Shaikh, P. Alerasool, E. Budina, J. Kang, N. Bhise, J. Ribas, A. Pourmand, A. Skardal, T. Shupe, C. E. Bishop, M. R. Dokmeci, A. Atala and A. Khademhosseini, *Proc. Natl. Acad. Sci. U. S. A.*, 2017, **114**, E2293–E2302.

84 L. E. Marshall, R. Koomullil, A. R. Frost and J. L. Berry, *Ann. Biomed. Eng.*, 2017, **45**, 1027–1038.

85 T. Miura and R. Tanaka, *Math. Modell. Nat. Phenom.*, 2009, **4**, 118–130.

86 Y. T. Wang, S. D. Mohammed, A. D. Farmer, D. Wang, N. Zarate, A. R. Hobson, P. M. Hellstrom, J. R. Semler, B. Kuo, S. S. Rao, W. L. Hasler, M. Camilleri and S. M. Scott, *Aliment. Pharmacol. Ther.*, 2015, **42**, 761–772.

87 C. E. Stevens and I. D. Hume, *Comparative physiology of the vertebrate digestive system*, Cambridge University Press, Cambridge New York, 2nd edn, 1995.

88 Z. J. Meng, W. Wang, X. Liang, W. C. Zheng, N. N. Deng, R. Xie, X. J. Ju, Z. Liu and L. Y. Chu, *Lab Chip*, 2015, **15**, 1869–1878.

89 C. Girabawe and S. Fraden, *Sens. Actuators, B*, 2017, **238**, 532–539.

90 L. G. Lowrey, *Am. J. Anat.*, 1911, **12**, 131.

91 C. C. Chou, *Fed. Proc.*, 1983, **42**, 1656–1657.

92 Y. M. Baraki, P. Traverso, H. A. Elariny and Y. Fang, *Surg. Technol. Int.*, 2010, **20**, 167–171.

93 D. J. L. John and W. Calvert, in *Muscle*, ed. E. N. O. J. A. Hill, Academic Press, 2012, ch. 6, vol. 1, pp. 57–66.